Natural Gas Density Measurements and the Impact of Accuracy on Process Design

Saif ZS. Al Ghafri[a], Fuyu Jiao[a], Thomas J. Hughes[b], Arash Arami-Niya[a,c], Xiaoxian Yang[a], Arman Siahvashi[a], Armand Karimi[a,d] and Eric F. May*[a]

[a]Fluid Science and Resources Division, Department of Chemical Engineering, University of Western Australia, Crawley, WA 6009, Australia

[b]*Resources Engineering Program, Department of Civil Engineering, Monash University, Clayton, Victoria 3800, Australia*

[c]*Discipline of Chemical Engineering, Western Australian School of Mines: Minerals, Energy and Chemical Engineering, Curtin University, GPO Box U1987, Perth, WA 6845, Australia*

[d]*IFP Energies Nouvelles, 1 et 4 Avenue de Bois-Préau, 92852, Rueil-Malmaison, France*

Corresponding author: Eric F. May. E-mail: Eric.May@uwa.edu.au

Abstract

The liquefaction of natural gas is an energy intensive processes, requiring 5% of the lower heating value. Key to estimating and optimizing these energy requirements are process simulations which rely upon calculated thermophysical properties of the natural gas. In particular, the prediction of thermophysical properties of natural gas mixtures at pressure-temperature conditions close to the mixture's critical point or cricondenbar is challenging but important as often natural gas processes operate close to these conditions. In this work, we present a comprehensive study of two natural gas related systems: (CH_4 + C_3H_8 + CO_2) and (CH_4 + C_3H_8 + C_7H_{16}) with *n*-heptane fractions up to 15 mol %. High accuracy measurements of densities, at temperatures from 200 K to 423 K and pressures up to 35 MPa are presented. The extensive experimental data collected for these mixtures were compared with the GERG-2008 equation of state, as implemented in the NIST software REFPROP. The relative

deviations of the measured densities from those calculated using the GERG-2008 model range between (-2 to 4) % for all mixtures, presenting a systematic dependent on mixture density and *n*-heptane content. Finally, a case study is presented that probes the impact of the accuracy of density on the pinch point in a simulated LNG heat exchanger. An uncertainty in the density of 1 % is shown to cause significant 30 % reduction in the minimum approach temperature difference, suggesting that accurate thermophysical property calculations are key to reducing over-design of processing plant.

Keywords: Methane + propane + *n*-heptane mixtures, Carbon dioxide, Density, Natural gas, Modelling

1. INTRODUCTION

Natural gas consists mainly of light hydrocarbons such as methane, ethane, propane as well as contaminants such as carbon dioxide, hydrogen sulfide and nitrogen [1]. It produces (50 to 60) % less CO_2 when burnt than coal and (15 to 20) % less greenhouse gases than gasoline when used in vehicles [2], making it central to the transition towards a low carbon-emissions society [3-9]. Prior to being fed into pipeline systems or liquefaction facilities [10], raw natural gas needs to be processed for it to meet product specifications. This involves separation of a series of undesirable components, like carbon dioxide, water, and hydrogen sulfide, and/or the recovery of more valuable components, for example, ethane, propane, butane, heavier hydrocarbons and helium [11-16]. The design of each stage in that transformation process uses predictions of the mixture's thermophysical properties as a function of temperature, pressure and composition [11, 12].

Many different models are available for predicting a mixture's thermophysical properties, each with varying complexity and accuracy. All, however, are anchored to measured data with the model's reliability generally decreasing as predictions go beyond the range of these anchoring data. The data required to confidently design gas processing equipment at operating conditions near the gas mixture's critical point are deficient, and ultimately lead to the over-design of plants, higher operating costs and less energy efficient processing [17]. To achieve better designs that work more effectively over a wider range of conditions, the gas industry needs new fundamental property data, both to resolve discrepancies in our current predictive capabilities and to extend them to the higher-pressure conditions characteristic of many new gas fields. This requires new and accurate thermophysical property data for natural gas mixtures be measured at conditions often considered inaccessible.

Thermodynamic models used in natural gas industry range from empirical and semi-empirical correlations, such as cubic equations of state (for example, PR76 [18] developed by Peng and Robinson), activity coefficients models and molecular-based models such as Statistical

79 Associating Fluid Theory (SAFT) [19]. Most recent efforts to improve LNG process simulations
80 have focussed on the use of complex equations of state [11-15] capable of more accurately
81 describing the VLE, density and other properties of multi-component fluid mixtures. These
82 include the GERG-2008 equation of state (EOS) by Kunz and Wagner [13] which is endorsed
83 by the International Organisation for Standardization (ISO 20765-2 and 20765-3) for natural
84 gas mixtures. All of the above models are tuned to existing experimental data from pure fluid
85 and binary mixtures [20]. Thus, in terms of ternary or multi-component gas mixtures, their
86 accuracy needs to be further tested with new high-quality experimental data [12]. Our recent
87 studies of thermodynamic properties such as phase equilibrium [14, 21-33], heat capacity [34,
88 35] and density [25, 36-38] clearly identified deficiencies in EOS commonly used by industry,
89 and in several of the archival literature data to which those models have been tuned [14].

90 Therefore, in this work, the density of gas and liquid phases at high pressures and over a
91 wide-range of temperatures, including near the mixture's critical point (where gas and liquid
92 become indistinguishable and the existing predictive fluid property models used by engineers
93 breakdown) were investigated. Here we present a comprehensive study of two prototype
94 systems of natural gas related gases: (CH_4 + C_3H_8 + CO_2) and (CH_4 + C_3H_8 + C_7H_{16});
95 comprising accurate measurements of the saturated-phase densities, and compressed-fluid
96 (single-phase) densities at temperature from 200 K to 423 K and pressures up to 35 MPa over
97 different ranges of compositions. These mixtures were chosen for investigation due to their
98 relevance for natural gas gathering, treating and processing equipment design and
99 optimization.

100 To our knowledge, no density data exists for the ternary mixtures considered in this work.
101 Some researchers have measured the density of natural gas related binary mixtures. Karimi
102 et al. [39] have measured the density of methane and propane mixtures at temperatures
103 between (256 and 422) K and pressure from (24 to 35) MPa using a magnetic suspension
104 densimeter. Yang et al. [40] have reported the density of methane and carbon dioxide gas
105 mixtures at temperatures between (300.15 to 313.15) K and pressures between (8 and 10)

MPa measured using a single-sinker densimeter. Richter et al. [41] developed a special densimeter and studied a synthetic five-component LNG mixture at temperatures between (105 to 135) K and pressures up to 8.1 MPa. Other researchers' studies can be found in Ref. [39-44]. We recently [36] extended the lowest operational temperature of a commercial vibrating tube densimeter (VTD) down to 203 K, calibrated using a robust physically based model [45]. The extended calibration was then employed for single-phase density measurements of a 0.95 methane + 0.05 propane mixture at a temperature of 203 K and pressure up to 35 MPa.

The experimental ranges of composition, temperature and pressure gathered in this work are summarized in **Table 1**. Mixtures 1, 2, and 3 correspond to (0.85 C1 + 0.10 C3 + 0.05 C7), (0.81 C1 + 0.09 C3 + 0.10 C7), and (0.71 C1 + 0.14 C3 + 0.15 C7), respectively. Mixture 4 corresponds to (0.640 C1 + 0.098 C3 + 0.261 CO_2).

Table 1. Summary of investigated ternary mixtures including composition, x, pressure range p and temperature range T.

Mixture	x_{C1}	x_{C3}	x_{C7}	x_{CO2}	T_{range}/K	p_{range}/MPa
	Single and bubble points density measurements					
Mixture 1	0.854	0.095	0.051	0	204 - 420	6 - 35
Mixture 2	0.809	0.090	0.101	0	203 - 420	7 - 35
Mixture 3	0.714	0.136	0.150	0	207 - 420	10 - 35
Mixture 4	0.640	0.098	0	0.262	273 - 421	10 - 35

These data were compared with the predictions of the GERG-2008 EOS [13] as implemented in the software REFPROP 10.0 [46]. The GERG-2008 EOS is a Helmholtz free energy model as a function of temperature, pressure and composition. In describing binary mixture thermodynamic properties, binary interaction parameters within reducing functions are adjusted to force agreement with experimental data. Equation (1) and (2) represent the

composition-dependent reducing functions for binary mixture density (ρ_r) and temperature (T_r), where $\beta_{v,ij}$, $\gamma_{v,ij}$, $\beta_{T,ij}$ and $\gamma_{T,ij}$ are adjusted binary parameters; $\rho_{c,i}$ and $T_{c,i}$ are critical density and critical temperature of pure component i.

$$\frac{1}{\rho_r(\bar{x})} = \sum_{i=1}^{N} x_i^2 \frac{1}{\rho_{c,i}} + \sum_{i=1}^{N-1} \sum_{j=i+1}^{N} 2x_i x_j \beta_{v,ij} \gamma_{v,ij} \cdot \frac{x_i + x_j}{\beta_{v,ij}^2 x_i + x_j} \cdot \frac{1}{8} \left(\frac{1}{\rho_{c,i}^{1/3}} + \frac{1}{\rho_{c,j}^{1/3}} \right)^3 \quad (1)$$

$$T_r(\bar{x}) = \sum_{i=1}^{N} x_i^2 T_{c,i} + \sum_{i=1}^{N-1} \sum_{j=i+1}^{N} 2x_i x_j \beta_{T,ij} \gamma_{T,ij} \cdot \frac{x_i + x_j}{\beta_{T,ij}^2 x_i + x_j} \left(T_{c,i} \cdot T_{c,j} \right)^{0.5} \quad (2)$$

Additionally, if a sufficient number of data were available at the time of the model's development, a departure function may be added to describe the specific binary to improve the accuracy of the model when describing that binary. The parameters and functions used for the description of binary mixtures relevant to this work are summarized in **Table 2**.

Table 2. Overview of GERG mixing functions for five binary mixtures

Binaries	Reducing functions				Departure function
	$\beta_{v,ij}$	$\gamma_{v,ij}$	$\beta_{T,ij}$	$\gamma_{T,ij}$	
C1 + C3	1.0048	1.0385	0.98968	1.0987	Yes
C1 + C7	0.96205	1.1567	0.97743	1.3799	None
C3 + C7	1.0	1.0796	1.0	1.05	None
C1 + CO_2	0.99952	1.0028	1.0226	0.97567	Yes
C3 + CO_2	0.9969	1.0476	1.0336	0.90877	None

2. Materials and Methods

2.1. Materials

The suppliers and supplier-analysed purities of all components used in this work are listed in **Table 3**. No further purification was attempted. The supplied (C_1 + C_3) gas mixtures for this

project had a certified standard relative uncertainty $u_r(x)$ of 1%. *n*-Heptane was degassed under vacuum before use.

Table 3. Source and purities of chemicals used in this work

Compound	Supplier	Mole fraction	CAS Number
Methane	Coregas	0.99999	74-82-8
Propane	Coregas	0.99995	74-98-6
Carbon Dioxide	Coregas	0.99995	124-38-9
n-Heptane	Sigma Aldrich	0.99	142-82-5
C_1 + C_3 mixtures	CAC Gas	0.8999 C1+ 0.1001 C3 0.8398 C1 + 0.1602 C3	N/A

2.2. Density-Vibrating tube densimeter

A vibrating tube densimeter [36] (Anton Paar, DMA HPM) was used to measure the density of the hydrocarbon ternary mixtures (C_1 + C_3 + C_7). Details regarding mixture preparation and compositional analysis, experimental setup, procedure, calibration and uncertainty are given in the Supplementary Information (SI). Initially a magnetic suspension densimeter was employed for this ternary system. However, due to the large volume of the magnetic suspension densimeter (≈ 100 ml) effects of de-mixing (due to the presence of a heavy component, heptane) were quite apparent and adversely affected the achievable repeatability of data acquired over long time period. Consequently, a vibrating tube densimeter (VTD) was employed to measure densities at pressures up to 140 MPa and temperatures up to 473.15 K using a U-shaped vibrating tube of 2 ml total volume. This relatively small size prevented the de-mixing of *n*-heptane and improved the reproducibility of our data. The overall standard uncertainty of the cell temperature was estimated to be 0.1 K based principally on temperature gradients and fluctuations. The standard uncertainty of the pressure measurement was estimated to be 0.01 MPa for the entire pressure range considered in the present work. Overall,

158 the combined standard relative uncertainty of densities measured in this work span between
159 (0.3 and 1.2) %, due mostly to the composition uncertainty.

160 2.3. Density-Magnetic-suspension balance

161 A commercial magnetic-suspension balance [39] developed primarily for sorption analysis
162 (type: IsoSORP, Rubotherm, Germany, and since 2016, TA instrument, USA) was used to
163 measure the density of the ternary system (0.640 C1+ 0.098 C_3 + 0.261 CO_2). The
164 experimental setup was as described previously [47] and further detailed in the Supplementary
165 Information including composition and uncertainty calculations. The overall standard
166 uncertainty of the cell temperature was estimated to be around 0.3 K considering gradients
167 along the measuring cell wall, the self-heating of the PRT, heat dissipation of the test leads,
168 temperature oscillations over time. The standard uncertainty of the pressure measurement
169 was estimated to be around 0.01 MPa for the entire pressure range considered in the present
170 work. The combined standard relative uncertainty in densities measured with this apparatus
171 ranged from (0.29 to 0.51) %.

172

173 3. Experimental Results and Discussion

174 3.1. Density of (C_1 + C_3 + C_7) mixtures

175 The vibrating tube densimeter was used to measure all the data acquired for methane +
176 propane + *n*-heptane mixtures. Along each isotherm, density measurements were performed
177 at every pressure for a minimum of 3 hours to check for drift with time. Additionally, a repeat
178 measurement was made at one pressure value to check the degree of reproducibility. The
179 experimental density results are presented in **Table 4**, together with the estimated standard
180 uncertainties. A summary of the pressure and temperature conditions of the measurements
181 is shown in **Fig. 1** for mixture 1 (0.854 C1 + 0.095 C3 + 0.051 C7), mixture 2 (0.809 C1 +
182 0.090 C3 + 0.101 C7) and mixture 3 (0.714 C1 + 0.136 C3 + 0.150 C7), along with the

predicted phase envelope for each mixture as calculated from the GERG-2008 EOS [13]. The cross symbols in **Fig. 1** correspond to the locations of the measurements used to determine the bubble point densities via the method of linear extrapolation, which is shown in **Fig. 2**. Overall a total of 99 density data were acquired from (170 to 548) kg·m^{-3}.

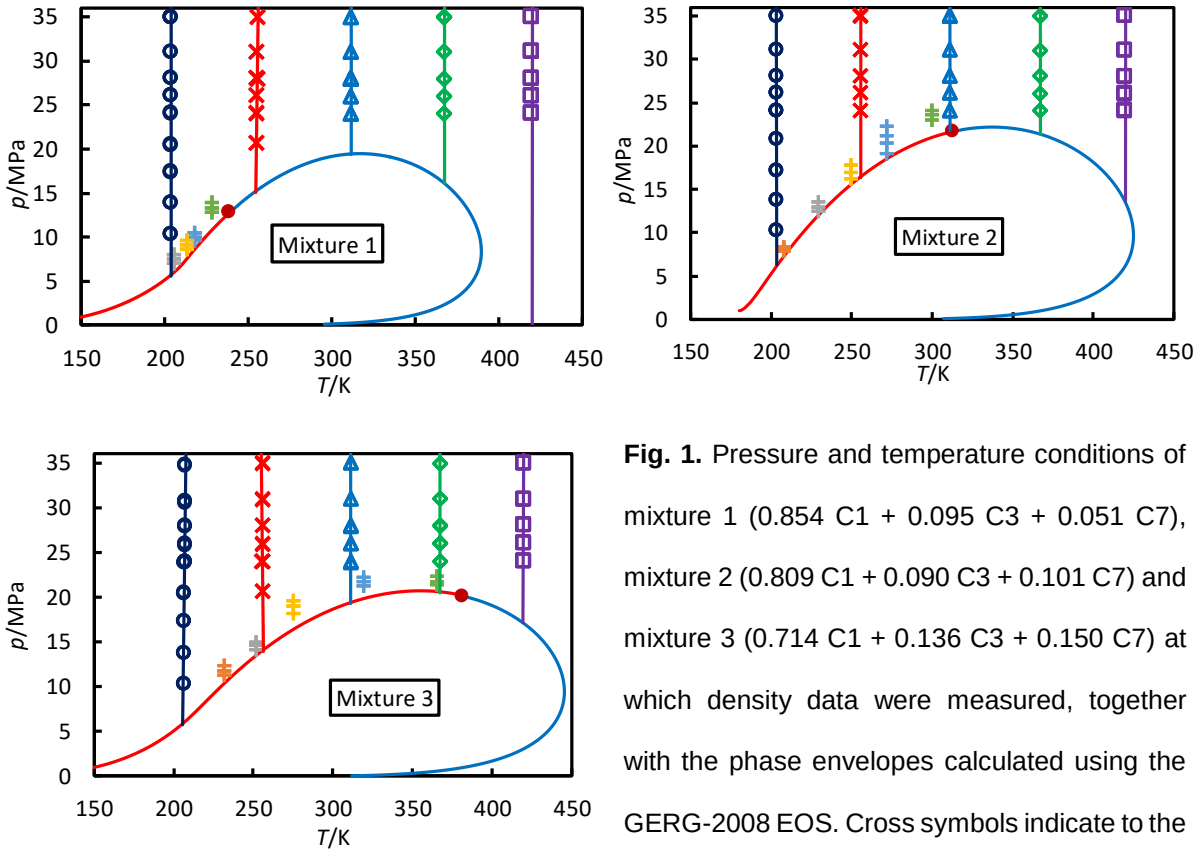

Fig. 1. Pressure and temperature conditions of mixture 1 (0.854 C1 + 0.095 C3 + 0.051 C7), mixture 2 (0.809 C1 + 0.090 C3 + 0.101 C7) and mixture 3 (0.714 C1 + 0.136 C3 + 0.150 C7) at which density data were measured, together with the phase envelopes calculated using the GERG-2008 EOS. Cross symbols indicate to the measurements used to estimate the bubble point densities.

Fig. 2 shows the measurements acquired to estimate the bubble point densities for mixtures 1, 2 and 3. The open symbols are the measurement points for each set of data and the straight lines are linear fits of those data extrapolated to the bubble point condition predicted by the GERG-2008 EOS. The filled black symbols are the calculated bubble point densities. A linear extrapolation with respect to pressure was deemed sufficient given the proximity of the data acquired to the saturation condition. Relative standard uncertainties of bubble point pressures as predicted by GERG-2008 EOS for binary mixtures (C1 + C3, C1 + C7, C3 + C7) were

reported to be (1 to 3) % [13]. Consequently, estimated relative uncertainties in calculated bubble pressures of ternary mixtures considered in this work were estimated to be 3.5%. This contributed largely to the overall relative standard uncertainties of bubble point densities, as shown in Table 4, which ranged from (0.5 to 1.8) %. However, this analysis does not include errors associated with linear extrapolation with respect to pressure.

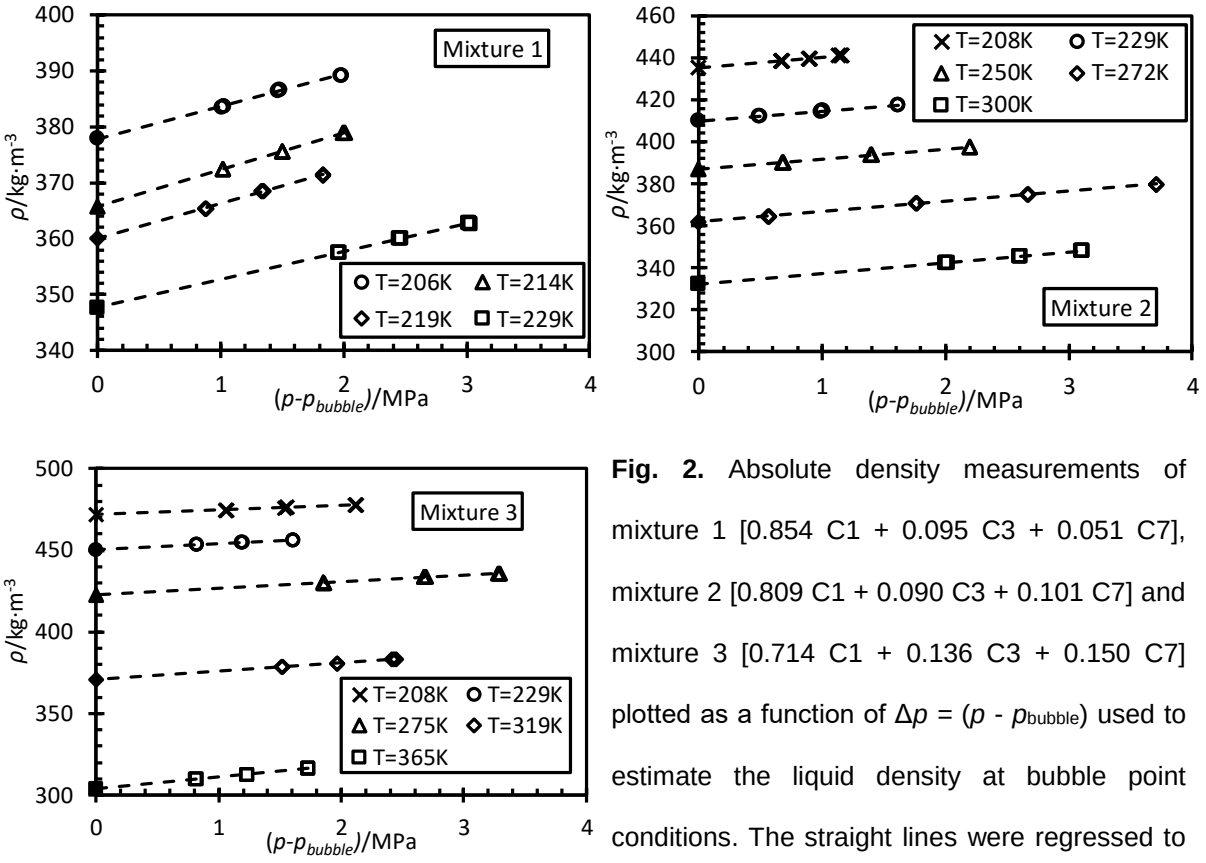

Fig. 2. Absolute density measurements of mixture 1 [0.854 C1 + 0.095 C3 + 0.051 C7], mixture 2 [0.809 C1 + 0.090 C3 + 0.101 C7] and mixture 3 [0.714 C1 + 0.136 C3 + 0.150 C7] plotted as a function of $\Delta p = (p - p_{bubble})$ used to estimate the liquid density at bubble point conditions. The straight lines were regressed to the measured (hollow) data points and used to estimate the density at the EOS-predicted bubble pressure (black filled symbols)

Density data measured for the single phase and bubble point conditions are shown in **Fig. 3, 4 and 5** for mixtures 1, 2 and 3, respectively. In these figures, the experimental density is plotted as a function of pressure for each mixture. Additionally, relative deviations of the measured densities from those calculated using the GERG-2008 model in REFPROP 10.0

are shown. The measured values for these mixtures follow the same trend as the predicted values. The relative deviations between the present measurements and the predicted values are between (- 1.5 to 2.5) %, (- 2 to 3.5) % and (0 to 4) % for mixture 1 (5 mol % n-heptane), mixture 2 (10 mol % n-heptane) and mixture 3 (15 mol % n-heptane), respectively. The deviations are systematically dependent on heptane content and pressures/densities. For each isothermal measurement, observed relative deviations increased with increasing pressures (densities). In addition, the highest relative deviations were always observed at the lowest isothermal measurements (207 K) for all three ternary mixtures.

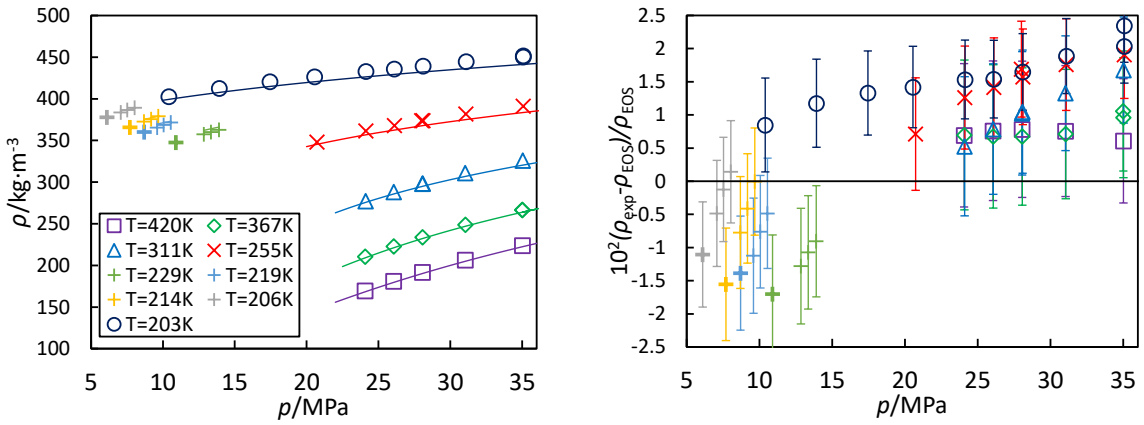

Fig. 3. Measured single-phase and bubble points densities for mixture 1 (0.854 C1 + 0.095 C3 + 0.051 C7) as a function of pressure, together with the densities calculated using the GERG-2008 EOS (solid lines) (left), and relative deviations of the measured densities from those calculated using the GERG-2008 model in REFPROP 10.0 (right).

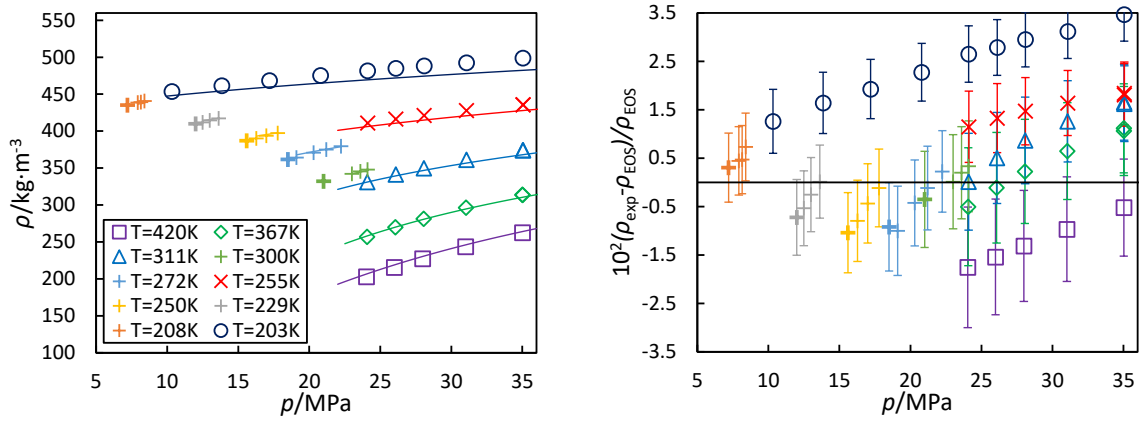

Fig. 4. Measured single-phase and bubble points densities for mixture 2 (0.809 C1 + 0.090 C3 + 0.101 C7) as a function of pressure, together with the calculated densities using GERG-2008 EOS (solid lines), and relative deviations of the measured densities from those calculated using the GERG-2008 model in REFPROP 10.0

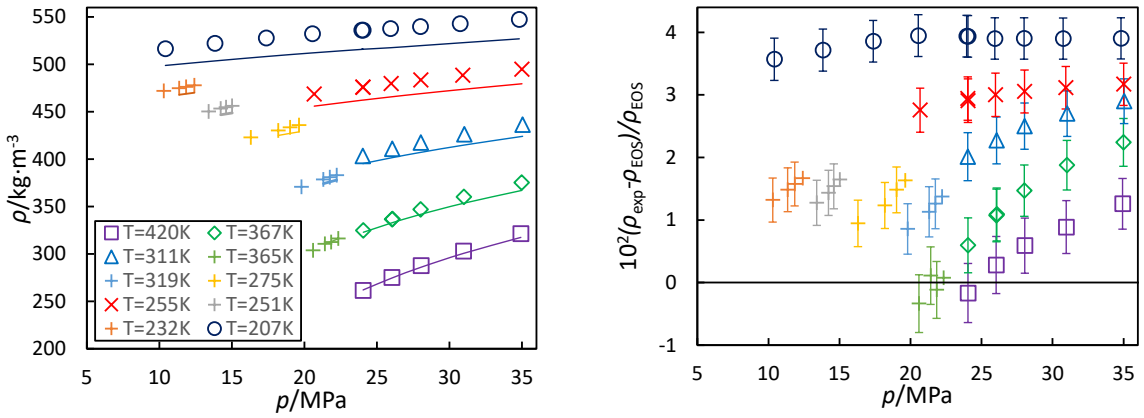

Fig. 5. Measured single-phase and bubble points densities for mixture 3 (0.714 C1 + 0.136 C3 + 0.150 C7) as a function of pressure, together with the calculated densities using GERG-2008 EOS (solid lines), and relative deviations of the measured densities from those calculated using the GERG-2008 model in REFPROP 10.0.

Overall, the relative deviations of the measured densities from those calculated using the GERG-2008 model span from (-2 to 4) % for all mixtures. The larger deviations observed in these mixtures reflect the absence of departure functions within the model for the component binaries of methane + *n*-heptane and propane + *n*-heptane (as previously indicated in **Table 2**). Developing departure functions for these binaries would require the acquisition of sufficient numbers of new data for them across a wide range of conditions. Unfortunately, there are limited reference quality data to reliably represent natural gas mixtures that contain heavier hydrocarbons (such as *n*-heptane) at high pressure and cryogenic conditions [20, 21]. For example, the density data sets used for the two important binary systems methane and propane, and methane and *n*-heptane in the GERG-2008 EOS have respective root mean square relative density deviations of (0.4 to 0.8) % and (0.9 to 2.5) % from the EOS [21].

The extensive set of literature data available for the methane + propane system were used to tune the binary interaction parameters and develop a departure function for this binary. As a result, the deviations of the data measured for this binary from the GERG-2008 EOS were generally within the experimental uncertainty, even though the new data were obtained at very different conditions to those used in the model development [36, 39]. However, for the binaries of methane + *n*-heptane and propane + *n*-heptane, no departure function was developed due to the limited available data. Thus, increased deviations can be expected for the mixtures containing *n*-heptane, as shown in this work.

Table 4. Measured single phase points and bubble points density data and their combined uncertainty $u_C(\rho)$ as a function of temperature *T* pressure *p* and composition for ternary Mixture 1 (0.854 C1 + 0.095 C3 + 0.051 C7), Mixture 2 (0.809 C1 + 0.090 C3 + 0.101 C7) and Mixture 3 (0.714 C1 + 0.134 C3 + 0.150 C7).

T/K	p/MPa	$x(CH_4)$	$x(C_3H_8)$	$x(C_7H_{16})$	ρ/kg·m^{-3}	$10^2(\rho-\rho_{GERG})/\rho_{GERG}$	$u_C(\rho)$/kg·m^{-3}
203.6	10.41	0.854	0.095	0.051	402.7	0.85	2.9
203.5	13.92	0.854	0.095	0.051	412.6	1.18	2.7
203.5	17.45	0.854	0.095	0.051	420.5	1.33	2.7
203.6	20.55	0.854	0.095	0.051	426.4	1.42	2.6
203.6	24.13	0.854	0.095	0.051	432.9	1.53	2.6
203.6	26.10	0.854	0.095	0.051	435.9	1.54	2.6
203.6	28.10	0.854	0.095	0.051	439.3	1.65	2.5
203.6	31.09	0.854	0.095	0.051	444.5	1.89	2.5
203.6	35.08	0.854	0.095	0.051	450.3	2.03	2.5
203.6	35.08	0.854	0.095	0.051	451.7	2.35	2.5
255.2	20.73	0.854	0.095	0.051	348.1	0.71	3.0
255.3	24.12	0.854	0.095	0.051	361.4	1.26	2.8
255.3	26.12	0.854	0.095	0.051	367.8	1.41	2.7
255.3	28.10	0.854	0.095	0.051	373.8	1.57	2.7

T/K	p/MPa	$x(CH_4)$	$x(C_3H_8)$	$x(C_7H_{16})$	ρ/kg·m^{-3}	$10^2(\rho-\rho_{GERG})/\rho_{GERG}$	$u_C(\rho)$/kg·m^{-3}
255.5	28.01	0.854	0.095	0.051	373.6	1.69	2.7
255.3	31.08	0.854	0.095	0.051	381.7	1.76	2.6
255.3	35.08	0.854	0.095	0.051	391.0	1.91	2.6
311.2	24.10	0.854	0.095	0.051	277.1	0.53	2.9
311.2	26.07	0.854	0.095	0.051	288.0	0.79	2.8
311.2	28.06	0.854	0.095	0.051	297.9	1.02	2.8
311.2	28.09	0.854	0.095	0.051	298.1	1.05	2.8
311.2	31.04	0.854	0.095	0.051	310.9	1.33	2.7
311.2	35.04	0.854	0.095	0.051	325.8	1.68	2.6
367.2	24.08	0.854	0.095	0.051	210.5	0.70	2.4
367.2	26.07	0.854	0.095	0.051	222.6	0.68	2.4
367.2	28.07	0.854	0.095	0.051	233.8	0.68	2.4
367.2	31.05	0.854	0.095	0.051	248.7	0.71	2.4
367.2	35.02	0.854	0.095	0.051	266.4	0.96	2.4
367.2	35.01	0.854	0.095	0.051	266.6	1.06	2.4
419.9	24.06	0.854	0.095	0.051	169.5	0.69	1.8
419.9	26.05	0.854	0.095	0.051	181.0	0.76	1.9
419.9	28.05	0.854	0.095	0.051	191.8	0.78	2.0
419.9	31.04	0.854	0.095	0.051	206.5	0.76	2.0
419.9	35.01	0.854	0.095	0.051	223.7	0.61	2.1
205.7	6.10	0.854	0.095	0.051	377.9*	-1.10	3.3
205.7	7.07	0.854	0.095	0.051	383.7	-0.48	3.1
205.7	7.53	0.854	0.095	0.051	386.6	-0.12	3.0
205.7	8.03	0.854	0.095	0.051	389.3	0.14	3.0
213.6	7.70	0.854	0.095	0.051	365.8*	-1.56	3.6
213.6	8.69	0.854	0.095	0.051	372.5	-0.77	3.1

T/K	p/MPa	$x(CH_4)$	$x(C_3H_8)$	$x(C_7H_{16})$	ρ/kg·m^{-3}	$10^2(\rho-\rho_{GERG})/\rho_{GERG}$	$u_C(\rho)$/kg·m^{-3}
213.6	9.18	0.854	0.095	0.051	375.6	-0.41	3.1
213.6	9.68	0.854	0.095	0.051	379.0	0.00	3.1
218.2	8.70	0.854	0.095	0.051	360.1*	-1.39	3.6
218.2	9.60	0.854	0.095	0.051	365.4	-1.12	3.2
218.2	10.06	0.854	0.095	0.051	368.5	-0.76	3.1
218.2	10.56	0.854	0.095	0.051	371.4	-0.48	3.1
228.5	10.90	0.854	0.095	0.051	347.7*	-1.70	3.6
228.5	12.85	0.854	0.095	0.051	357.5	-1.28	3.1
228.5	13.35	0.854	0.095	0.051	360.1	-1.07	3.1
228.5	13.91	0.854	0.095	0.051	362.8	-0.90	3.0
203.5	10.33	0.809	0.090	0.101	453.7	1.26	3.0
203.4	13.85	0.809	0.090	0.101	461.7	1.64	2.9
203.4	17.20	0.809	0.090	0.101	468.5	1.93	2.9
203.4	20.79	0.809	0.090	0.101	475.5	2.27	2.8
203.5	24.10	0.809	0.090	0.101	481.8	2.65	2.8
203.4	26.11	0.809	0.090	0.101	485.1	2.79	2.8
203.4	28.10	0.809	0.090	0.101	488.4	2.95	2.8
203.4	31.07	0.809	0.090	0.101	492.7	3.12	2.8
203.5	35.05	0.809	0.090	0.101	498.9	3.47	2.7
255.5	24.12	0.809	0.090	0.101	411.0	1.15	3.0
255.5	26.11	0.809	0.090	0.101	416.3	1.33	3.0
255.5	28.10	0.809	0.090	0.101	421.2	1.47	2.9
255.5	31.07	0.809	0.090	0.101	427.8	1.64	2.9
255.5	35.05	0.809	0.090	0.101	435.7	1.81	2.8
255.5	35.06	0.809	0.090	0.101	435.8	1.84	2.8
311.2	24.10	0.809	0.090	0.101	331.2	0.01	3.3

T/K	p/MPa	$x(CH_4)$	$x(C_3H_8)$	$x(C_7H_{16})$	ρ/kg·m^{-3}	$10^2(\rho-\rho_{GERG})/\rho_{GERG}$	$u_C(\rho)$/kg·m^{-3}
311.2	26.10	0.809	0.090	0.101	341.2	0.50	3.2
311.2	28.08	0.809	0.090	0.101	349.9	0.86	3.1
311.2	31.07	0.809	0.090	0.101	361.3	1.26	3.0
311.2	35.05	0.809	0.090	0.101	374.2	1.65	2.9
311.2	35.06	0.809	0.090	0.101	374.1	1.62	2.9
367.2	24.07	0.809	0.090	0.101	256.9	-0.50	3.1
367.2	26.06	0.809	0.090	0.101	269.8	-0.11	3.1
367.2	28.06	0.809	0.090	0.101	281.3	0.22	3.0
367.2	31.05	0.809	0.090	0.101	296.5	0.64	3.0
367.2	35.02	0.809	0.090	0.101	313.8	1.12	2.9
367.2	35.03	0.809	0.090	0.101	313.7	1.06	2.9
419.9	24.03	0.809	0.090	0.101	203.0	-1.76	2.5
419.9	25.99	0.809	0.090	0.101	215.5	-1.54	2.6
419.9	27.99	0.809	0.090	0.101	227.3	-1.32	2.6
419.9	31.01	0.809	0.090	0.101	243.6	-0.97	2.6
419.9	35.02	0.809	0.090	0.101	262.6	-0.52	2.6
207.8	7.20	0.809	0.090	0.101	435.1*	0.30	3.3
207.8	7.92	0.809	0.090	0.101	438.5	0.44	3.1
207.8	8.15	0.809	0.090	0.101	439.2	0.47	3.1
207.8	8.40	0.809	0.090	0.101	440.9	0.73	3.1
229.3	12.00	0.809	0.090	0.101	409.8*	-0.72	3.7
229.3	12.50	0.809	0.090	0.101	412.0	-0.54	3.2
229.3	13.00	0.809	0.090	0.101	414.5	-0.25	3.2
229.3	13.62	0.809	0.090	0.101	417.2	0.01	3.1
249.8	15.60	0.809	0.090	0.101	386.9*	-1.04	4.1
249.8	16.27	0.809	0.090	0.101	390.1	-0.80	3.3

T/K	p/MPa	$x(CH_4)$	$x(C_3H_8)$	$x(C_7H_{16})$	ρ/kg·m^{-3}	$10^2(\rho-\rho_{GERG})/\rho_{GERG}$	$u_C(\rho)$/kg·m^{-3}
249.8	16.99	0.809	0.090	0.101	393.7	-0.44	3.2
249.8	17.79	0.809	0.090	0.101	397.3	-0.12	3.2
272.2	18.50	0.809	0.090	0.101	361.8*	-0.92	4.6
272.2	19.10	0.809	0.090	0.101	364.3	-1.00	3.4
272.2	20.30	0.809	0.090	0.101	370.8	-0.43	3.3
272.2	21.20	0.809	0.090	0.101	375.0	-0.12	3.2
272.2	22.25	0.809	0.090	0.101	379.7	0.22	3.2
299.9	21.00	0.809	0.090	0.101	332.1*	-0.35	5.0
299.9	23.00	0.809	0.090	0.101	342.3	0.01	3.3
299.9	23.60	0.809	0.090	0.101	345.5	0.20	3.3
299.9	24.10	0.809	0.090	0.101	347.9	0.33	3.3
206.5	10.41	0.714	0.136	0.150	516.7	3.57	1.7
206.5	13.83	0.714	0.136	0.150	522.4	3.72	1.8
206.5	17.37	0.714	0.136	0.150	527.9	3.86	1.8
206.5	20.55	0.714	0.136	0.150	532.3	3.95	1.8
206.7	24.04	0.714	0.136	0.150	536.2	3.94	1.8
206.6	23.95	0.714	0.136	0.150	536.2	3.94	1.8
207.1	25.94	0.714	0.136	0.150	537.8	3.90	1.8
207.1	28.00	0.714	0.136	0.150	540.0	3.90	1.8
206.9	30.74	0.714	0.136	0.150	543.1	3.90	1.8
206.6	34.81	0.714	0.136	0.150	547.5	3.90	1.8
255.4	20.68	0.714	0.136	0.150	468.7	2.76	1.6
255.4	24.03	0.714	0.136	0.150	476.1	2.94	1.7
255.4	24.05	0.714	0.136	0.150	475.9	2.91	1.7
255.4	25.98	0.714	0.136	0.150	479.9	3.00	1.7
255.4	28.03	0.714	0.136	0.150	483.6	3.05	1.7

T/K	p/MPa	$x(CH_4)$	$x(C_3H_8)$	$x(C_7H_{16})$	ρ/kg·m^{-3}	$10^2(\rho-\rho_{GERG})/\rho_{GERG}$	$u_C(\rho)$/kg·m^{-3}
255.4	30.93	0.714	0.136	0.150	488.5	3.11	1.7
255.4	35.00	0.714	0.136	0.150	494.8	3.17	1.7
310.9	24.03	0.714	0.136	0.150	403.4	2.01	1.5
310.9	26.06	0.714	0.136	0.150	410.8	2.27	1.5
310.9	28.02	0.714	0.136	0.150	417.4	2.50	1.5
310.9	31.03	0.714	0.136	0.150	426.2	2.70	1.5
310.9	35.04	0.714	0.136	0.150	436.3	2.90	1.6
367.2	24.05	0.714	0.136	0.150	324.9	0.59	1.4
367.2	26.05	0.714	0.136	0.150	336.6	1.07	1.4
367.2	26.07	0.714	0.136	0.150	336.8	1.09	1.4
367.2	28.01	0.714	0.136	0.150	346.9	1.47	1.4
367.2	31.01	0.714	0.136	0.150	360.3	1.88	1.4
367.2	34.99	0.714	0.136	0.150	375.3	2.24	1.4
419.8	24.04	0.714	0.136	0.150	261.6	-0.17	1.2
419.8	26.03	0.714	0.136	0.150	275.4	0.28	1.3
419.8	28.05	0.714	0.136	0.150	287.7	0.59	1.3
419.8	30.97	0.714	0.136	0.150	303.2	0.89	1.3
419.8	34.93	0.714	0.136	0.150	321.4	1.26	1.3
231.6	10.30	0.714	0.136	0.150	472.0*	1.32	2.0
231.6	11.36	0.714	0.136	0.150	474.9	1.48	1.7
231.6	11.85	0.714	0.136	0.150	476.3	1.58	1.7
231.6	12.42	0.714	0.136	0.150	477.9	1.67	1.7
251.6	13.40	0.714	0.136	0.150	450.4*	1.27	2.3
251.6	14.23	0.714	0.136	0.150	453.4	1.43	1.6
251.6	14.60	0.714	0.136	0.150	454.8	1.54	1.6
251.6	15.02	0.714	0.136	0.150	456.2	1.65	1.6

T/K	p/MPa	$x(CH_4)$	$x(C_3H_8)$	$x(C_7H_{16})$	ρ/kg·m^{-3}	$10^2(\rho-\rho_{GERG})/\rho_{GERG}$	$u_C(\rho)$/kg·m^{-3}
275.0	16.30	0.714	0.136	0.150	423.0*	0.95	2.8
275.1	18.19	0.714	0.136	0.150	430.3	1.23	1.6
275.1	19.02	0.714	0.136	0.150	433.7	1.48	1.6
275.0	19.62	0.714	0.136	0.150	436.0	1.63	1.6
319.3	19.80	0.714	0.136	0.150	370.9*	0.86	3.8
319.3	21.31	0.714	0.136	0.150	378.6	1.13	1.5
319.3	21.76	0.714	0.136	0.150	380.9	1.26	1.5
319.3	22.22	0.714	0.136	0.150	383.2	1.37	1.5
365.1	20.60	0.714	0.136	0.150	303.9*	-0.34	5.3
365.1	21.42	0.714	0.136	0.150	310.7	0.11	1.4
365.1	21.84	0.714	0.136	0.150	312.6	-0.12	1.4
365.1	22.33	0.714	0.136	0.150	316.3	0.08	1.4

* The bubble point result is obtained by the method of linear extrapolation

Uncertainties in temperatures: $u(T)$ = 0.1 K, pressure: $u(p)$ = 0.01 MPa and composition: $u(x_1)$ =0.008, $u(x_2)$ =0.008, $u(x_3)$ =0.002.

3.2. Density of (C_1 + C_3 + CO_2) mixture

Single-phase density measurements at temperatures of (273.3, 298.2, 323.0, 347.5, 368.6, 400.2 and 420.5) K and pressures up to 35 MPa were obtained for mixture 4 (0.640 C1 + 0.098 C3 + 0.261 CO_2), using a magnetic suspension densimeter [39]. The experimental density results are given in **Table 5**, together with the estimated standard uncertainties. **Fig. 6** shows the location in the (ρ, p) and (p, T) planes of the measurements conducted in this work for the ternary mixture, relative to its phase envelope, which was calculated using the GERG-2008 EOS [13] as implemented in the software REFPROP 10.0 [46]. Additionally, relative deviations of the measured densities from those calculated using the GERG-2008 are shown in **Fig.7**. Overall, a total of 47 density data were acquired from (83 to 456) kg·m^{-3}. The relative deviations of the measured densities from those calculated using the GERG-2008

EOS [13] span from (-0.3 to +0.7) %, which is nearly within the combined uncertainty of the measurements. Extensive literature data for the methane + propane and methane + carbon dioxide were available and used to tune the binary interaction parameters and to develop departure functions for these binaries. As a result, the deviations of the data measured from GERG-2008 EOS are generally within the experimental and model uncertainty.

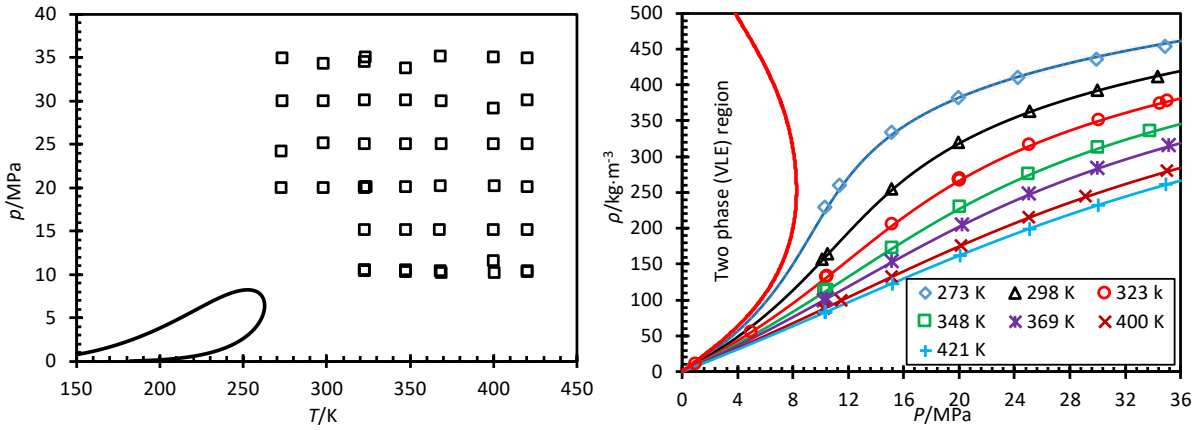

Fig. 6. Pressure**,** density and temperature conditions of the ternary mixture (0.640 C1 + 0.098 C3 + 0.261 CO_2) density data measured in this work, together with its phase envelope calculated using the GERG-2008 EOS.

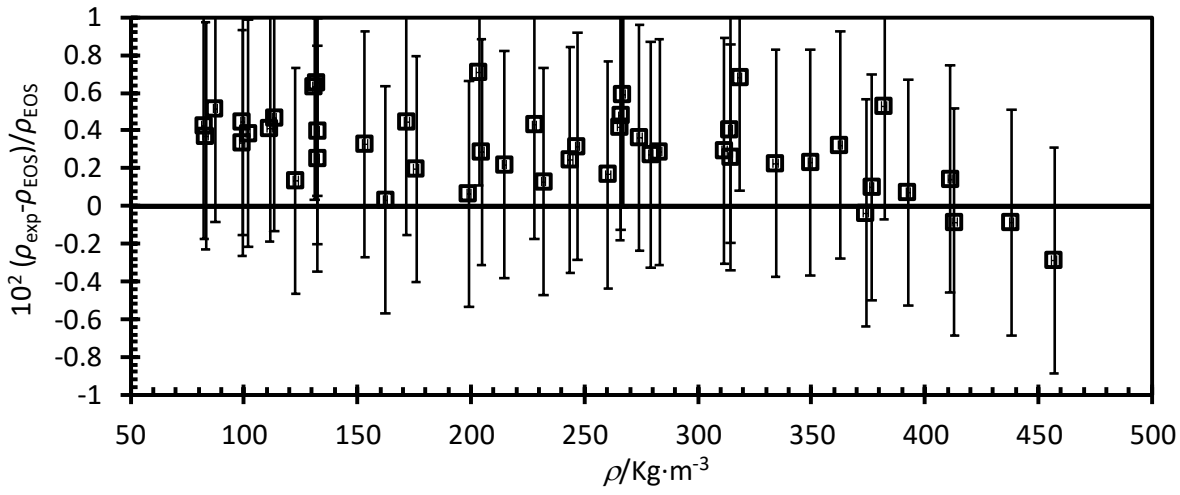

Fig. 7. Relative deviations of the measured densities from those calculated using the GERG-2008 model in REFPROP 10.0.

278 **Table 5.** Experimental density data and combined standard (k = 1) uncertainties for the (0.6401 C1 +
279 0.0984 C3 + 0.2615 CO_2) mixture and their relative deviations from values calculated with the GERG-
280 2008 equation of state.

T/K	p/MPa	ρ/kg·m^{-3}	$10^2(\rho-\rho_{GERG})/\rho_{GERG}$	$u_C(\rho)$/kg·m^{-3}
273.07	19.93	384.1	0.53	0.41
273.04	24.21	411.8	0.14	0.35
273.60	29.94	437.8	-0.09	0.31
273.49	34.89	455.7	-0.29	0.29
298.03	19.95	320.6	0.68	0.46
298.25	25.11	363.8	0.32	0.38
298.22	30.01	392.9	0.07	0.34
298.17	34.32	412.8	-0.08	0.32
322.95	10.42	131.9	0.63	0.48
322.93	15.17	205.0	0.71	0.51
322.96	20.10	268.6	0.59	0.46
323.01	25.06	315.5	0.40	0.40
323.01	30.09	350.4	0.23	0.36
323.03	35.06	376.9	0.10	0.33
322.94	10.50	133.1	0.66	0.49
322.96	10.50	132.8	0.40	0.50
323.68	20.10	266.9	0.42	0.46
323.00	20.01	267.2	0.48	0.46
323.02	34.53	373.9	-0.04	0.33
347.31	10.30	111.9	0.41	0.42
347.48	15.16	172.5	0.44	0.45
347.48	20.09	229.0	0.43	0.44
347.41	25.00	275.2	0.36	0.40
347.52	30.07	312.5	0.29	0.36
347.45	33.80	335.0	0.23	0.34
347.38	10.47	113.9	0.46	0.42

T/K	p/MPa	ρ/kg·m^{-3}	$10^2(\rho-\rho_{GERG})/\rho_{GERG}$	$u_C(\rho)$/kg·m^{-3}
368.95	10.22	99.8	0.45	0.39
367.90	15.15	153.7	0.33	0.41
368.18	20.22	205.3	0.28	0.41
368.58	25.04	247.7	0.32	0.39
368.52	29.95	283.9	0.29	0.36
368.50	35.13	315.3	0.26	0.34
368.07	10.41	102.2	0.38	0.39
400.30	10.20	87.8	0.52	0.36
400.29	15.14	132.7	0.25	0.38
400.40	20.14	176.3	0.19	0.38
400.28	25.04	215.3	0.22	0.37
400.29	29.15	244.3	0.24	0.36
400.17	35.02	280.1	0.27	0.34
400.03	11.49	99.5	0.33	0.37
420.30	10.30	82.7	0.43	0.35
420.50	15.16	122.8	0.13	0.36
420.18	20.08	162.3	0.03	0.37
420.36	25.06	199.2	0.07	0.36
420.57	30.08	232.3	0.13	0.35
420.37	34.94	260.8	0.17	0.33
420.31	10.40	83.4	0.37	0.35

Uncertainties in temperatures: $u(T)$ = 0.3 K, pressure: $u(p)$ = 0.01 MPa and composition: $u(x)$ = 0.001.

4. Case study - Impact of measured properties on LNG heat exchanger design

The impact of thermodynamic property uncertainty on process simulations has been studied by multiple authors, concluding that a reference quality data for multicomponent hydrocarbon mixtures would improve the reliability of process simulations [48-50]. Dauber and Span [12]

examined the influence of different properties models on the simulation of the LNG liquefaction process and LNG transport. They concluded that GERG-2008 EOS provides the highest potential for accurate calculations of the thermodynamic properties of natural gas such as density, heat capacity and enthalpy. However, in their work, the composition of the LNG considered was only representative of the feed entering the main cryogenic heat exchange (MCHE) and did not include heavy hydrocarbons (C_6+) or vapor-liquid equilibrium data and only focused on the liquefaction process.

Here we present a case study of heat exchanger design to demonstrate the importance of the accuracy of the fluid thermophysical properties in the LNG process. The purpose of the heat exchanger is to cool and liquefy a quasi-LNG stream (vapour phase) to the outlet temperature $T_{\mathrm{LNG,out}}$ = 178 K (liquid phase). The quasi-LNG stream is a binary (methane + ethane) mixture with a methane mole fraction of 0.89 and with a normalized mole flowrate of $\dot{m}_{\mathrm{LNG}}$ = 1.00 mol/s. The refrigerant stream is a ternary (methane + ethane + nitrogen) mixture with an inlet temperature $T_{\mathrm{refr,in}}$, a flowrate $\dot{m}_{\mathrm{refr}}$ and designated mixture compositions x_{refr} of the refrigerant stream (x_{refr} = [x_{C1}, x_{C2}, x_{N2}]). The enthalpy profile of the quasi-LNG stream h_{LNG} can be calculated as a function of the temperature of the refrigerant stream T_{refr} by:

$$
\begin{aligned}
&h_{\mathrm{LNG}}\left(T_{\mathrm{LNG},j}\right)=\left[h_{\mathrm{refr}}\left(T_{\mathrm{refr},j}\right)-h_{\mathrm{refr}}\left(T_{\mathrm{refr},i}\right)\right]\cdot\frac{\dot{m}_{\mathrm{refr}}}{\dot{m}_{\mathrm{LNG}}}+h_{\mathrm{LNG}}\left(T_{\mathrm{LNG},i}\right)\\
&T_{\mathrm{refr},i}=T_{\mathrm{refr,in}},\ \text{and}\ T_{\mathrm{LNG},i}=T_{\mathrm{LNG,out}}\ \text{when}\ i=0\\
&T_{\mathrm{refr},j}-T_{\mathrm{refr},i}=1\ \mathrm{K}
\end{aligned}
\qquad (3)
$$

Here the heat exchanger was broken into segments such that in each segment the temperature changes of the refrigerant is 1 K and we assume that there are negligible heat loss and pressure loss in both streams. In equation (3), the enthalpy of the refrigerant stream $h_{\mathrm{refr}}(T_{\mathrm{refr},i})$ at each temperature $T_{\mathrm{refr},i}$, and the enthalpy of the quasi-LNG stream at the outlet $h_{\mathrm{LNG}}(T_{\mathrm{LNG,out}})$ can be estimated using the GERG-2008 EOS as implemented in the software package REFPROP 10.0. Then, according to the calculated $h_{\mathrm{LNG}}(T_{\mathrm{LNG},j})$, the temperature of

the quasi-LNG stream $T_{LNG,j}$ can be determined. Therefore, the temperature profile of the quasi-LNG stream T_{LNG} as a function of the temperature of the refrigerant stream T_{refr} can be determined. An example with x_{refr} = [0.63, 0.32, 0.05], $T_{refr,in}$ = 169 K and $\dot{m}_{refr}$ = 1.95 mol/s in the refrigerant stream is depicted in **Fig. 8(a).**

The example as shown in **Fig. 8(a)** is a result of trial-and-error in choosing values of x_{refr}, $T_{refr,in}$ and $\dot{m}_{refr}$ so that T_{LNG} is higher than T_{refr} but not by much; in this way the heat exchanger between the two streams works efficiently. There is a pinch point, or minimum approach temperature, where the temperature difference between the two streams $\Delta T = T_{LNG} - T_{refr}$ reaches the smallest value with ΔT_{pinch} = 4.1 K. The value ΔT_{pinch} is very sensitive to the values of the fluid thermophysical properties. To demonstrate this, we present two other cases in **Fig. 8(b),** one with a 1.0 % less flowrate ($\dot{m}_{refr}$ = 1.93 mol/s) and another with a change of 0.01 mole fraction in the mixture composition (x_{refr} = [0.64, 0.31, 0.05]) in the refrigerant stream. The first case which corresponds to a relative uncertainty in density calculation of 1.0 % shows a reduction of ΔT_{pinch} to 2.9 K or almost 30 % which is significant. The second case results in a negative non-physical ΔT_{pinch} of −0.5 K which is unacceptable in the heat exchanger design. Therefore, in order to avoid a negative value of ΔT_{pinch} in the heat exchanger, the design margin is high; however, if the uncertainty in the density and enthalpy calculation could be reduced, the design margin could be reduced and thus the energy consumption and the CAPEX and OPEX can be better optimized. The actual effect of uncertain properties such as density in LNG heat exchanger design is even larger, because errors in calculated densities also effect Reynolds and Nusselt numbers used in the heat exchanger design calculations.

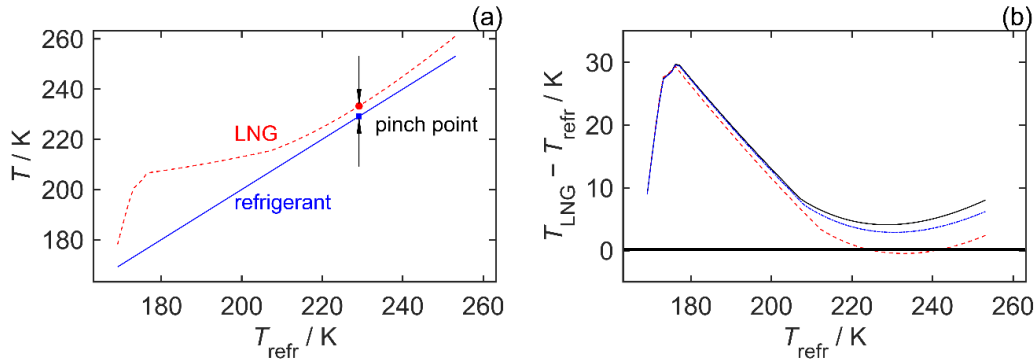

Fig. 8(a) The temperature of the quasi-LNG stream T_{LNG} (red dashed curve) and the refrigerant stream T_{refr} in a heat exchanger. (b) The temperature difference between the quasi-LNG stream and the refrigerant stream. The quasi-LNG stream is a binary (methane + ethane) mixture with a methane mole fraction of 0.89 and with a flowrate of 1.00 mol/s in both figures. The refrigerant streams are ternary (methane + ethane + nitrogen) mixtures with: mole fraction of (0.63, 0.32, 0.05) and flowrate of 1.95 mol/s for (a) and the black solid curve in (b); mole fraction of (0.63, 0.32, 0.05) and flowrate of 1.93 mol/s for the blue dashed dotted curve in (b); and mole fraction of (0.64, 0.31, 0.05) and flowrate of 1.95 mol/s for the red dashed curve in (b).

5. Conclusion

In this work, we present a comprehensive study of two prototype systems: (CH_4 + C_3H_8 + CO_2) and (CH_4 + C_3H_8 + C_7H_{16}); in the last of these the *n*-heptane content was up to 15 mol %, comprising accurate measurements of the saturated-phase densities and compressed-fluid (single phase) densities, at temperature from 200 K to 423 K and pressures up to 35 MPa over different ranges of compositions. The extensive experimental data collected for these mixtures were compared with the GERG-2008 EOS. The comparison shows that the relative deviations of the measured densities from those calculated using the GERG-2008 model span between (-2 to 4) % for all mixtures, exhibiting a systematic dependency on mixture density and *n*-heptane content, which is attributed to the limited experimental data available for the binary systems methane + *n*-heptane and propane + *n*-heptane. The case study on an LNG heat exchanger with a change in the density of 1 % resulted in an almost 30 % change in the minimum approach temperature, demonstrating the importance of accurate thermophysical properties to allow better equipment designs to lower energy consumption and operating costs. Current levels of uncertainty in the ISO standard for prediction of heavy hydrocarbon mixtures thermophysical properties cause predictions to be unreliable and may typically lead to significant equipment over design in industry.

6. Acknowledgment

This work was funded by the Gas Processors Association through project GPA-102 and Australian Research Council through IC150100019.

7. References

[1] Wang X, Economides M. CHAPTER 1 - Natural Gas Basics. Advanced Natural Gas Engineering: Gulf Publishing Company; 2009. p. 1-34.

[2] Chen J, Yu J, Ai B, Song M, Hou W. Determinants of global natural gas consumption and import–export flows. Energy Economics. 2018.

[3] Lin B, Kuang Y. Natural gas subsidies in the industrial sector in China: National and regional perspectives. Appl Energy. 2020;260:114329.

[4] Chen Y, Xu X, Koch T. Day-ahead high-resolution forecasting of natural gas demand and supply in Germany with a hybrid model. Appl Energy. 2020;262:114486.

[5] Yuan Z, Ou X, Peng T, Yan X. Life cycle greenhouse gas emissions of multi-pathways natural gas vehicles in china considering methane leakage. Appl Energy. 2019;253:113472.

[6] Obringer R, Mukherjee S, Nateghi R. Evaluating the climate sensitivity of coupled electricity-natural gas demand using a multivariate framework. Appl Energy. 2020;262:114419.

[7] García Kerdan I, Jalil-Vega F, Toole J, Gulati S, Giarola S, Hawkes A. Modelling cost-effective pathways for natural gas infrastructure: A southern Brazil case study. Appl Energy. 2019;255:113799.

[8] Czubinski FF, Al Ghafri SZS, Hughes TJ, Stanwix PL, May EF. Viscosity of a $[xCH_4 + (1 - x)C_3H_8]$ mixture with $x = 0.8888$ at temperatures between (203 and 424) K and pressures between (2 and 31) MPa Fuel. 2018;225:563-72.

[9] Al Ghafri SZS, Czubinski FF, May EF. Viscosity Measurements of (CH_4 + C_3H_8 + CO_2) Mixtures at Temperatures between (203 and 420) K and Pressures between (3 and 31) MPa. Fuel. 2018;231:187-96.

[10] Wang X, Economides M. CHAPTER 5 - Natural Gas Transportation—Pipelines and Compressed Natural Gas. Advanced Natural Gas Engineering: Gulf Publishing Company; 2009. p. 171-208.

[11] Dauber F, Span R. Achieving higher accuracies for process simulations by implementing the new reference equation for natural gases. Comput Chem Eng. 2012;37:15-21.

[12] Dauber F, Span R. Modelling liquefied-natural-gas processes using highly accurate property models. Appl Energy. 2012;97:822-7.

[13] Kunz O, Wagner W. The GERG-2008 Wide-Range Equation of State for Natural Gases and Other Mixtures: An Expansion of GERG-2004. J Chem Eng Data. 2012;57:3032-91.

[14] May EF, Guo JY, Oakley JH, Hughes TJ, Graham BF, Marsh KN, et al. Reference Quality Vapor–Liquid Equilibrium Data for the Binary Systems Methane + Ethane, + Propane, + Butane, and + 2-Methylpropane, at Temperatures from (203 to 273) K and Pressures to 9 MPa. J Chem Eng Data. 2015;60:3606-20.

[15] Rowland D, Hughes TJ, May EF. Extending the GERG-2008 Equation of State: Improved Departure Function and Interaction Parameters for (Methane + Butane). J Chem Thermodyn. 2016;doi: http://dx.doi.org/10.1016/j.jct.2016.01.005.

[16] Rufford TE, Smart S, Watson GCY, Graham BF, Boxall J, Diniz da Costa JC, et al. The removal of CO2 and N2 from natural gas: A review of conventional and emerging process technologies. J Pet Sci Eng. 2012;94-95:123-54.

[17] Laskowski LM, Kandil M, May E, Trebble M, Trengove R, Trinter J, et al. Reliable thermodynamic data for improving LNG scrub column design. 2008.

[18] Peng D-Y, Robinson DB. A New Two-Constant Equation of State. Ind Eng Chem Fundam. 1976;15:59-64.

[19] Chapman WG, Gubbins KE, Jackson G, Radosz M. SAFT: Equation-of-state solution model for associating fluids. Fluid Phase Equilib. 1989;52:31-8.

[20] Rowland D, Hughes TJ, May EF. Extending the GERG-2008 equation of state: Improved departure function and interaction parameters for (methane + butane). The Journal of Chemical Thermodynamics. 2016;97:206-13.

[21] Hughes TJ, Kandil ME, Graham BF, Marsh KN, Huang SH, May EF. Phase Equilibrium Measurements of (Methane + Benzene) and (Methane + Methylbenzene) at Temperatures from (188 to 348) K and Pressures to 13 MPa. J Chem Thermodyn. 2015;85:141-7.

[22] Kandil ME, Thoma MJ, Syed T, Guo J, Graham BF, Marsh KN, et al. Vapor-Liquid Equilibria Measurements of the Methane + Pentane and Methane + Hexane Systems at Temperatures from (173 to 330) K and Pressures to 14 MPa. J Chem Eng Data. 2011;56:4301-9.

[23] Kandil ME, May EF, Graham BF, Marsh KN, Trebble MA, Trengove RD, et al. Vapor-Liquid Equilibria Measurements of Methane + 2-Methylpropane (Isobutane) at Temperatures from (150 to 250) K and Pressures to 9 MPa. J Chem Eng Data. 2010;55:2725-31.

[24] Al Ghafri SZS, Trusler JPM. Phase equilibria of (Methylbenzene + Carbon dioxide + Methane) at elevated pressure: Experiment and modelling. J Supercrit Fluids. 2019;145:1-9.

[25] Al Ghafri SZS, Rowland D, Akhfash M, Arami-Niya A, Khamphasith M, Xiao X, et al. Thermodynamic properties of hydrofluoroolefin (R1234yf and R1234ze(E)) refrigerant mixtures: Density, vapour-liquid equilibrium, and heat capacity data and modelling. Int J Refrig. 2019;98:249-60.

[26] Souza LFS, Al Ghafri SZS, Trusler JPM. Measurement and modelling of the vapor–liquid equilibrium of (CO2 + CO) at temperatures between (218.15 and 302.93) K at pressures up to 15 MPa. The Journal of Chemical Thermodynamics. 2018;126:63-73.

[27] Sanchez-Vicente Y, Tay WJ, Al Ghafri SZ, Trusler JPM. Thermodynamics of carbon dioxide-hydrocarbon systems. Appl Energy. 2018;220:629-42.

[28] Al Ghafri SZS, Maitland GC, Trusler JPM. Phase Behavior of the System (Carbon Dioxide + n-Heptane + Methylbenzene): A Comparison between Experimental Data and SAFT-γ-Mie Predictions. J Chem Eng Data. 2017;62:2826-36.

435 [29] Al Ghafri SZ, Forte E, Galindo A, Maitland GC, Trusler JM. Experimental and Modeling
436 Study of the Phase Behavior of (Heptane+ Carbon Dioxide+ Water) Mixtures. J Chem Eng
437 Data. 2015;60:3670-81.
438 [30] Al Ghafri SZ, Maitland GC, Trusler JPM. Experimental and modeling study of the phase
439 behavior of synthetic crude oil+CO2. Fluid Phase Equilib. 2014;365:20-40.
440 [31] Al Ghafri SZ, Forte E, Maitland GC, Rodriguez-Henríquez JJ, Trusler JM. Experimental
441 and modeling study of the phase behavior of (methane+ CO2+ water) mixtures. J Phys Chem
442 B. 2014;118:14461-78.
443 [32] Al Habsi SSA, Al Ghafri SZS, Bamagain R, Trusler JPM. Experimental and modelling
444 study of the phase behavior of (methyl propanoate + carbon dioxide) at temperatures between
445 (298.15 and 423.15) K and pressures up to 20 MPa. Fluid Phase Equilib. 2020;519:112653.
446 [33] Al Ghafri SZS, Hughes TJ, Perez F, Baker CJ, Siahvashi A, Karimi A, et al. Phase
447 equilibrium studies of high-pressure natural gas mixtures with toluene for LNG applications.
448 Fluid Phase Equilib. 2020;518:112620.
449 [34] Xiao X, Oakley J, Al Ghafri SZS, Hughes T, Rowland D, Hnedkovsky L, et al. Isobaric
450 heat capacities of a methane (1) + propane (2) mixture by differential scanning calorimetry at
451 near-critical and supercritical conditions. Fuel. 2021;289:119840.
452 [35] Xiao X, Al Ghafri SZS, Rowland D, Hughes TJ, Hnedkovsky L, Hefter G, et al. Isobaric
453 heat capacity measurements of natural gas model mixtures (methane + n-heptane) and
454 (propane + n-heptane) by differential scanning calorimetry at temperatures from 313 K to
455 422 K and pressures up to 31 MPa. Fuel. 2021;296:120668.
456 [36] Jiao F, Al Ghafri SZS, Hughes TJ, May EF. Extended calibration of a vibrating tube
457 densimeter and new reference density data for a methane-propane mixture at temperatures
458 from (203 to 423) K and pressures to 35 MPa. J Mol Liq. 2020;310:113219.
459 [37] Sanchez-Vicente Y, Tay WJ, Al Ghafri SZ, Efika EC, Trusler JPM. Density and Phase
460 Behavior of the CO_2 + Methylbenzene System in Wide Ranges of Temperatures and
461 Pressures. Ind Eng Chem Res 2020;59:7224-37.

462 [38] Akhfash M, Al Ghafri SZS, Rowland D, Hughes TJ, Tsuji T, Tanaka Y, et al. Liquid and
463 Vapor Viscosities of Binary Refrigerant Mixtures Containing R1234yf or R1234ze(E). J Chem
464 Eng Data. 2019.
465 [39] Karimi A, Hughes TJ, Richter M, May EF. Density Measurements of Methane + Propane
466 Mixtures at Temperatures between (256 and 422) K and Pressures from (24 to 35) MPa. J
467 Chem Eng Data. 2016;61:2782-90.
468 [40] Yang X, Wang Z, Li Z. Accurate density measurements on a binary mixture (carbon
469 dioxide + methane) at the vicinity of the critical point in the supercritical state by a single-sinker
470 densimeter. Fluid Phase Equilibria. 2016;418:94-9.
471 [41] Richter M, Kleinrahm R, Lentner R, Span R. Development of a special single-sinker
472 densimeter for cryogenic liquid mixtures and first results for a liquefied natural gas (LNG). The
473 Journal of Chemical Thermodynamics. 2016;93:205-21.
474 [42] Yang X, Richter M, Wang Z, Li Z. Density Measurements on Binary Mixtures (Nitrogen +
475 Carbon Dioxide and Argon + Carbon Dioxide) at Temperatures from (298.15 to 423.15) K with
476 Pressures from (11 to 31) MPa using a Single-Sinker Densimeter. The Journal of Chemical
477 Thermodynamics. 2015;91:17-29.
478 [43] Yang X, Wang Z, Li Z. Accurate Density Measurements on Ternary Mixtures (Carbon
479 Dioxide + Nitrogen + Argon) at Temperatures from (323.15 to 423.15) K with Pressures from
480 (3 to 31) MPa using a Single-Sinker Densimeter. Journal of Chemical & Engineering Data.
481 2015;60:3353-7.
482 [44] Patil P, Ejaz S, Atilhan M, Cristancho D, Holste JC, Hall KR. Accurate density
483 measurements for a 91% methane natural gas-like mixture. The Journal of Chemical
484 Thermodynamics. 2007;39:1157-63.
485 [45] May EF, Tay WJ, Nania M, Aleji A, Al Ghafri S, Martin Trusler JP. Physical Apparatus
486 Parameters and Model for Vibrating Tube Densimeters at Pressures to 140 MPa and
487 Temperatures to 473 K. Rev Sci Instrum. 2014;85:095111.

[46] Lemmon EW, Huber ML, McLinden MO. NIST Standard Reference Database 23: Reference Fluid Thermodynamic and Transport Properties-REFPROP. 10.0.0 ed. Gaithersburg, MD: National Institute of Standards and Technology; 2013.

[47] Arami-Niya A, Rufford TE, Dresp G, Al Ghafri S, Jiao F, May EF. Measurements of helium adsorption on natural clinoptilolite at temperatures from (123.15 to 423.15) K and pressures up to 35 MPa. Sep Purif Technol. 2019;223:1-9.

[48] Carlson EC. Don't gamble with physical properties for simulations. Chemical Engineering Progress. 1996;92:35-46.

[49] Harvey AH, Laesecke A. Fluid properties and new technologies: Connecting design with reality. Chemical Engineering Progress. 2002;98:34-41.

[50] Rhodes CL. Process simulation revolution: Thermophysical property needs and concerns. Journal of Chemical and Engineering Data. 1996;41:947-50.